AIAA JOURNAL
Vol. 33, No. 7, July 1995

Direct Numerical Simulation of Turbulent Transport with Uniform Wall Injection and Suction

Yasushi Sumitani* and Nobuhide Kasagi†
University of Tokyo, Bunkyo-ku, Tokyo 113, Japan

A direct numerical simulation (DNS) of the fully developed turbulent channel flow and heat transfer with uniform wall injection and suction was carried out. The Reynolds number, which was based on the channel half-width and the friction velocity averaged on the two walls, was set to be 150, whereas the Prandtl number was 0.71. The walls were assumed to be kept at isothermal but different temperatures. With any buoyancy effect neglected, temperature was considered as a passive scalar. The computation was executed on sufficiently dense grid points by using a spectral method. The statistics obtained include the mean velocity and temperature, Reynolds stresses, and turbulent heat fluxes. Each term in the budget equations of the second-order velocity and temperature correlations and of their destruction rates was also calculated. It is found that the injection decreases the friction coefficient, but tends to stimulate the near-wall turbulence activity so that the Reynolds stresses and turbulent heat fluxes are increased, whereas the suction has an inverse influence.

Nomenclature

C_f = friction coefficient, $\tau_w/(\rho U_b^2/2)$
c_p = specific heat at constant pressure
F = mass flux ratio, v_0/U_b
F'' = mass flux ratio, v_0/U_m
h = heat transfer coefficient, $q_w/(\Theta_w - \Theta_b)$
k = turbulent kinetic energy, $\overline{u_i'u_i'}/2$, or wave number
k_θ = variance of temperature fluctuation, $\overline{\theta'^2}/2$
Nu = Nusselt number, $2h\delta/\lambda$
Pr = molecular Prandtl number, ν/α
p = pressure
q = heat flux
Re_b = Reynolds number, $2U_b\delta/\nu$
Re_τ = Reynolds number, $u_\tau\delta/\nu$
U, V = mean velocities
U_b = bulk mean velocity
U_m = maximum mean velocity
u, v, w = velocity components in the x, y, and z directions
u_τ = friction velocity, $\sqrt{\tau_w/\rho}$
x, y, z = streamwise, wall-normal, and spanwise coordinates
δ = channel half-width
ε = dissipation rate of k
ε_θ = dissipation rate of k_θ
Θ = mean temperature
Θ_b = bulk mean temperature
θ = temperature
θ_τ = friction temperature, $q_w/\rho c_p u_\tau$
λ = thermal conductivity
ν = kinematic viscosity
ρ = density
τ_w = wall shear stress averaged on two walls, unless otherwise noted

Subscripts

$()_I$ = on injection side
$()_{rms}$ = root-mean-square value
$()_S$ = on suction side
$()_w$ = wall value
$()_0$ = without injection and suction

Superscripts

$()'$ = fluctuating component
$()^+$ = normalized by the wall variables on each wall
$()^*$ = normalized by u_τ, ν, and θ_τ
$\overline{()}$ = ensemble average over x-z plane and time

Introduction

SHEAR flow turbulence control techniques are of great importance in a variety of engineering applications.[1] Among them, injection or suction of fluid normal to a wall surface should be one of the most effective methods. For instance, injection is applied to turbine-blade film cooling[2] and it is also known to bring about surface drag reduction effectively.[3] On the other hand, suction is often used as an aerodynamic flow control technique to prevent laminar-to-turbulent boundary-layer transition as well as flow separation. Up to the present, considerable effort has been made to accumulate knowledge of the effects of injection and suction on turbulent wall-bounded shear flow and heat transfer. The surface friction and heat transfer in turbulent boundary layers with and without acceleration and deceleration were extensively investigated and reported in Refs. 4–8. The mean velocity and temperature distributions were also measured to analyze and model the turbulent momentum and heat transport in the presence of injection and suction.[6–8] Furthermore, the measurement of velocity and temperature fluctuations was recently undertaken in an attempt to study the detailed flow structures of a turbulent boundary layer[9] and of a pipe flow[10] with wall suction. Despite these research efforts, many aspects of heat and mass transfer mechanisms affected by injection and suction still remain unknown due to the complexity of near-wall turbulence; and even basic turbulence statistics, particularly in the near-wall region, are insufficient for further refinement of the existing turbulence closure models.

With recent developments in computers and computational fluid dynamics, numerical simulations have been performed for this class of turbulent flows. Moin,[11] Piomelli,[12] and Piomelli et al.[13] carried out the large eddy simulations (LES) of turbulent channel flow with injection and suction using the no-slip or approximate wall boundary conditions. They confirmed the previous experimental findings on the behavior of the flowfield with injection and suction and, in addition, presented data of Reynolds stresses.[12,13] A direct numerical simulation (DNS) of an asymptotic turbulent boundary layer over

Received May 18, 1993; presented as Paper 93-3101 at the AIAA 24th Fluid Dynamics Conference, Orlando, FL, July 6–9, 1993; revision received Sept. 27, 1994; accepted for publication Sept. 27, 1994.

*Graduate Student, Department of Mechanical Engineering, Hongo 7-3-1; currently at MITI, Kasumigaseki 1-3-1, Chiyoda-ku, Tokyo 100, Japan.
†Professor, Department of Mechanical Engineering, Hongo 7-3-1. Member AIAA.

a flat plate with suction was recently reported in Ref. 14, wherein the Reynolds stress budgets were also first reported.

In this paper, a DNS of the fully developed turbulent channel flow and heat transfer with uniform injection and suction at the two opposite walls was carried out in order to establish a comprehensive database including various turbulence statistics and their budgets. In addition, instantaneous flowfields are visualized to get an indication of how the wall injection and suction alter the turbulent transport mechanisms.

Numerical Procedures

The flow geometry and the coordinate system are shown in Fig. 1. The Reynolds number Re_τ, based on wall friction velocity u_τ and channel half-width δ, was set to be 150. Note that u_τ is calculated from the wall shear stress averaged on the two walls. The resultant bulk Reynolds number Re_b was 4357. The Prandtl number of fluid was assumed to be 0.71. Referring to the numerical procedure used by Kim et al.,[15] a fourth-order partial differential equation for v, a second-order partial differential equation for the wall-normal component of vorticity, and the continuity equation were used to solve the flowfield. A spectral method was adopted with Fourier series in the x and z directions and a Chebyshev polynomial expansion in the y direction. The flow and thermal fields were assumed to be fully developed, so that the periodic boundary conditions were imposed at the periods of $5\pi\delta$ and $2\pi\delta$ (2356 and 942 in wall units) in the x and z directions, respectively. Chebyshev polynomials up to 96th order and 128×128 Fourier modes in wave number space were used to resolve all essential turbulent scales on the computational grid. The collocation grid used to compute the nonlinear terms in physical space had 1.5 times finer resolution in each direction to remove aliasing errors. For time integration, the second-order Adams-Bashforth and Crank-Nicolson schemes were adopted for the nonlinear and viscous terms, respectively. The time increment was $0.12\nu/u_\tau^2$.

The ordinary no-slip boundary condition was imposed on the u and w components at the walls, but a constant mean velocity was given to the wall-normal component ($V = v_0$). Its dimensionless value $v_0^*(= v_0/u_\tau)$ was set to be 0.05 and the resultant mass flux ratios were $F = 0.00344$ and $F'' = 0.00287$, respectively. The two walls were assumed to be kept at different but constant temperatures without fluctuations, and any buoyancy effect was neglected.

A program code developed in Refs. 16 and 17 was modified and used. The computation was carried out on a HITAC-S820/80 supercomputer system at the Computer Center of the University of Tokyo. For one time step advancement, 5.3-s CPU time was required. Initially the computation was continued until both flow and thermal fields were judged to have reached a fully developed state. Then, in order to obtain various turbulence statistics and their budgets, ensemble averages over space and time were taken for 7200 ν/u_τ^2 (60,000 time steps) and 3600 ν/u_τ^2 (30,000 time steps) in the flow and thermal field, respectively.

Because of an extremely heavy computational load, the computation was not repeated with changing the number of numerical grids systematically. However, the statistics and instantaneous flow patterns of the turbulent velocity field without injection and suction were extensively compared to available experimental and simulation data including the DNS of Ref. 15. In general, the agreement was very good, and the Reynolds number dependence of the statistics was confirmed to be consistent. As for the thermal field, global parameters, such as the heat transfer coefficient and the mean temperature profile, were confirmed[16] to be in good agreement with the available experimental data. In the energy spectra of velocity and

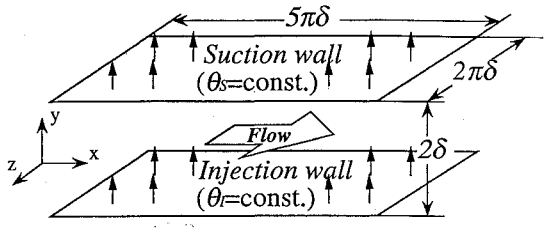

Fig. 1 Flow geometry and coordinate system.

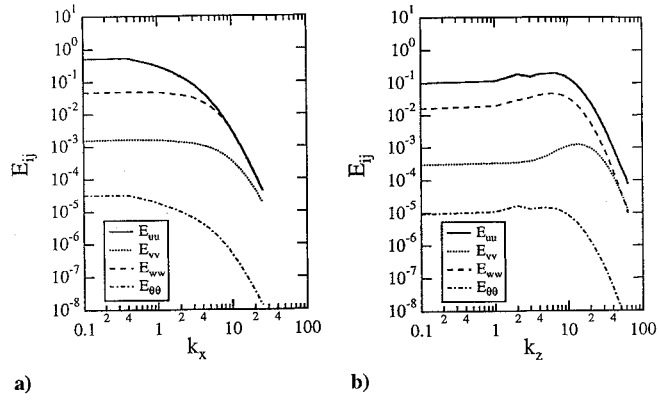

Fig. 2 Energy spectra at $y/\delta = -0.97$ (near the injection wall).

temperature fluctuations (typical examples near the injection wall are shown in Fig. 2), there is no noticeable energy accumulation at high wave numbers that should be evidence of insufficient numerical resolution. As shown later, it is found that the momentum conservation is confirmed, and even the dissipation budgets are smooth; these add to the confidence of the present simulation.

Results and Discussion

Mean Flow Parameters and Turbulent Statistics

The distribution of mean velocity U normalized by U_b is shown in Fig. 3, where the results of Kuroda et al.[17] and Piomelli et al.[13] are also included for comparison. In Ref. 17, a DNS of ordinary fully developed channel flow ($F = 0$) was made at the same Reynolds number of $Re_\tau = 150$, whereas in Ref. 13 LESs were carried out at a much higher Reynolds number, $Re_\tau = 833$, with a larger mass flux ratio, $F'' = 0.004$ (or, approximately, $F = 0.0049$). It is seen that with the mass flux ratio increased, the degree of asymmetry is more enhanced, and the position of the maximum velocity is shifted toward the suction-side wall. Presently, the maximum velocity, which is $U_m^* = 17.4$, is located at $y/\delta = 0.48$. Note that the near-wall profile of Ref. 13 is fuller than the others, because the former Reynolds number is higher.

As has been experimentally reported, the mean velocity gradient near the wall becomes gentler on the injection side although steeper on the suction side, if compared with that of $F = 0$. The friction coefficient C_f is 6.29×10^{-3} and 1.27×10^{-2} with injection and suction, respectively, whereas without them $C_{f0} = 8.64 \times 10^{-3}$. Therefore, with only 0.34% of the bulk flow rate, C_f decreases by 27% on the injection wall and increases by 47% on the suction wall. These are compared with the previous experimental,[5,7] LES,[13] and DNS[14] results in Fig. 4, where the friction coefficient C_f'' is defined based on the maximum (or freestream) velocity instead of the bulk mean velocity. Good agreement is obtained between the present DNS and the experimental data.[5,7]

The near-wall mean velocity distributions of U^+ are shown in Fig. 5, where comparison is made with the LES results[13] with a larger mass flux ratio. Note that the superscript $(\,)^+$ denotes a value nondimensionalized by the friction velocity on each wall and, hereafter, y represents the distance from each of the two walls. When compared with the case[17] of $F = 0$, both mean velocity profiles obtained by the LES[17] and the present DNS shift upward on the injection side, although downward on the suction side. Thus, these simulations give a consistent variation of the logarithmic velocity profiles. It is also evident in the present results that a wider logarithmic layer is established with injection, but with suction it no longer exists. These results should be useful for testing and improving various versions of the generalized law of the wall which have been developed, e.g., Refs. 5 and 12.

The dimensionless root-mean-square velocity fluctuations in the near-wall regions are shown in Fig. 6. On the injection side (Fig. 6a), the fluctuations are activated. The maximum streamwise fluctuation, which is increased by about 25%, is located closer ($y^+ = 13$) to the wall than in the case without injection ($y^+ = 14$). The wall-normal and spanwise components, v'_{rms} and w'_{rms}, are also increased by about 60%. However, as shown in Fig. 6b, all of the fluctuations

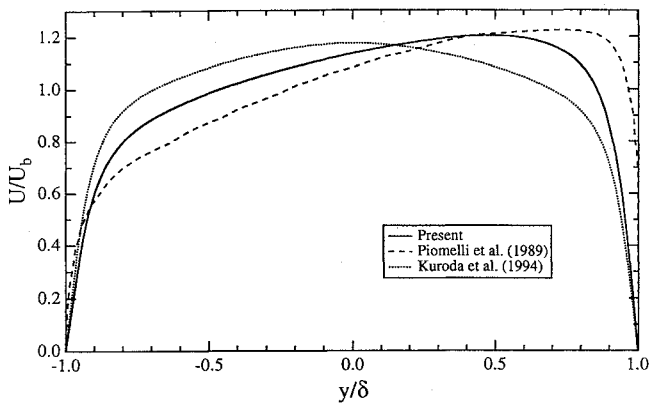

Fig. 3 Mean velocity profile.

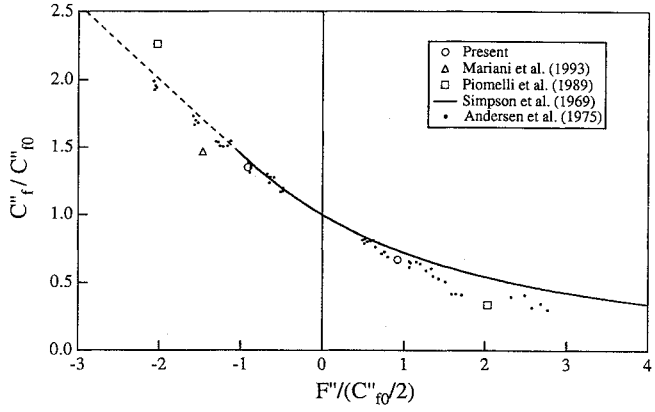

Fig. 4 Ratio of friction coefficients with and without wall mass flux.

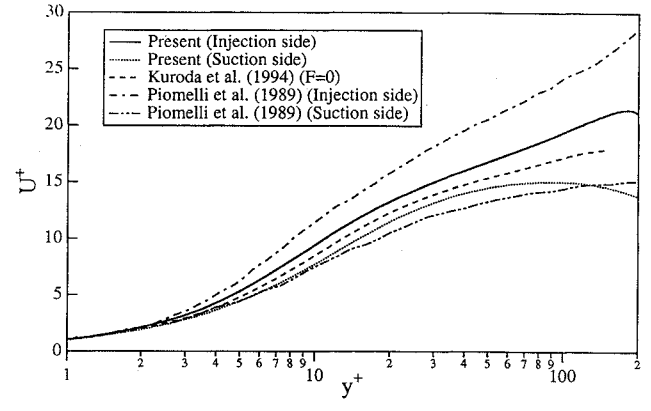

Fig. 5 Mean velocity profile near the wall.

are decreased on the suction side; $v'_{\rm rms}$ no longer has a peak and remains less than half of that without suction in the region of $y^+ < 60$. The maximum values of $u'_{\rm rms}$ and $w'_{\rm rms}$ are smaller by about 35% than those without suction. The maximum $u'_{\rm rms}$ is moved farther away ($y^+ = 16$) from the wall.

The near-wall stress balances are shown in Fig. 7. The averaged momentum equation of the fully developed flow leads to

$$1 - \left(\frac{u_\tau}{u_{\tau_l}}\right)^2 \frac{y^+}{Re_{\tau_l}} = \frac{\partial U^+}{\partial y^+} - \overline{u'^+v'^+} - U^+ \cdot v_0^+ \qquad (1)$$

$$1 - \left(\frac{u_\tau}{u_{\tau_s}}\right)^2 \frac{y^+}{Re_{\tau_s}} = \frac{\partial U^+}{\partial y^+} - \overline{u'^+v'^+} - U^+ \cdot v_0^+ \qquad (2)$$

for the injection and suction walls, respectively. Hence, the sum of the viscous stress, the Reynolds stress, and the convective momentum transport on the right-hand side (RHS) of Eqs. (1) and (2) should balance with the pressure gradient on the left-hand side (LHS) and

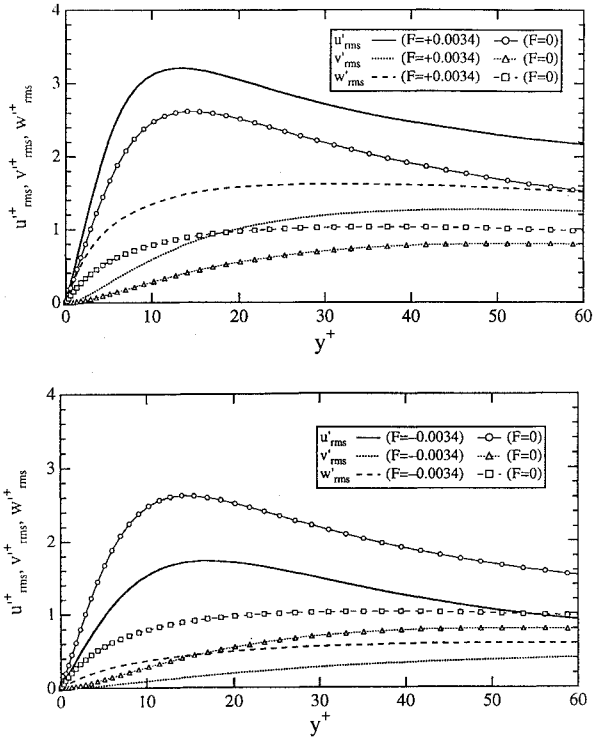

Fig. 6 Root-mean-square velocity fluctuations: a) injection side and b) suction side.

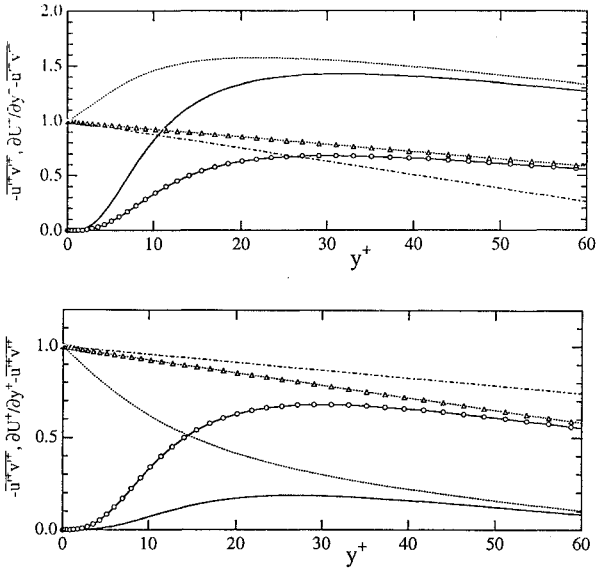

Fig. 7 Stress component distributions: a) injection side and b) suction side. $-\overline{u'^+v'^+}$: ——, $F = \pm 0.0034$; —○—, $F = 0$; $\partial U^+/\partial y^+ - \overline{u'^+v'^+}$: ·····, $F = \pm 0.0034$; ···Δ···, $F = 0$; $\partial U^+/\partial y^+ - \overline{u'^+v'^+} - U^+ \times v_0^+$: —·—·, $F = \pm 0.0034$.

be linear with respect to y^+. Note that the convective transport should be zero if $F = 0$. As seen in Figs. 7a and 7b, the RHSs of Eqs. (1) and (2) actually show linear distributions and, hence, the flowfield is judged to be fully developed. The total shear stress is zero at $y/\delta = 0.53$, which is close to the maximum velocity point ($y/\delta = 0.48$). On the injection side, the Reynolds shear stress increases twice that of $F = 0$, and the viscous stress also increases slightly, whereas negative convective transport takes place. As a result, the sum of momentum flux is a little smaller than that of $F = 0$. However, the total flux is larger on the suction side, where the Reynolds stress decreases to about a quarter, and the viscous stress also decreases, whereas the convective transport is largely positive.

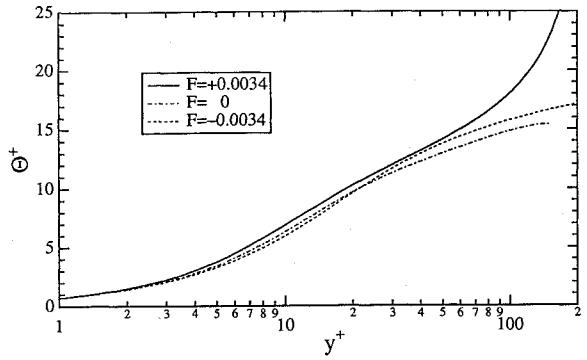

Fig. 8 Mean temperature profile.

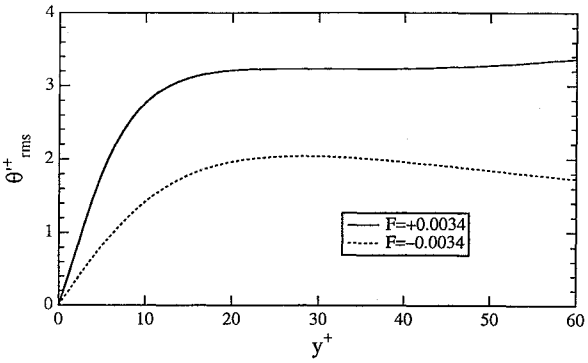

Fig. 9 Root-mean-square temperature fluctuation.

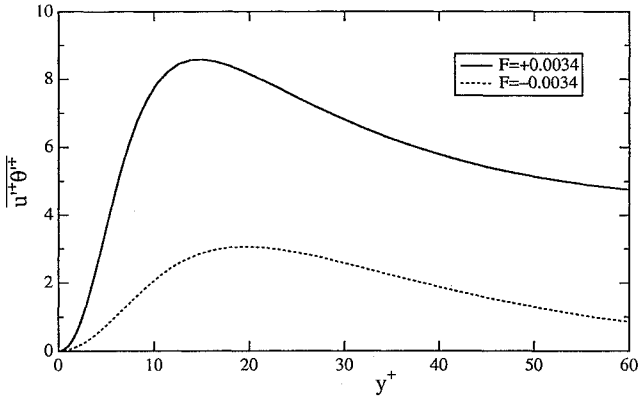

Fig. 10 Streamwise turbulent heat flux.

Figure 8 shows the mean temperature profile normalized by the friction temperature on each wall. The curve denoted as $F = 0$ in this figure is that in a channel flow which is heated with a constant wall heat flux at the two walls.[16] Despite the clear change in the mean velocity profiles with injection and suction, the temperature profile seems to change only moderately. The Nusselt number obtained by the present simulation is 3.48 and 15.3 on the injection and suction walls, respectively, whereas the value for $F = 0$ estimated from Ref. 18 is 13.1. The dimensionless root-mean-square temperature fluctuation is shown in Fig. 9. It is evident that, like the velocity fluctuations, the temperature fluctuation is increased by injection although decreased by suction.

Figure 10 shows the distributions of streamwise turbulent heat flux with injection and suction. The relative difference in the magnitudes is greatly enhanced if compared with the rms temperature fluctuations, and this suggests that the correlation between the velocity and temperature fluctuations is also influenced considerably. The wall-normal turbulent heat flux is shown in Fig. 11. For the fully developed channel flow between isothermal walls, the heat flux balance is derived as follows

$$1 = \frac{1}{Pr}\frac{\partial \Theta^+}{\partial y^+} - \overline{v'^+\theta'^+} - v_0^+ \cdot \Theta^+ \tag{3}$$

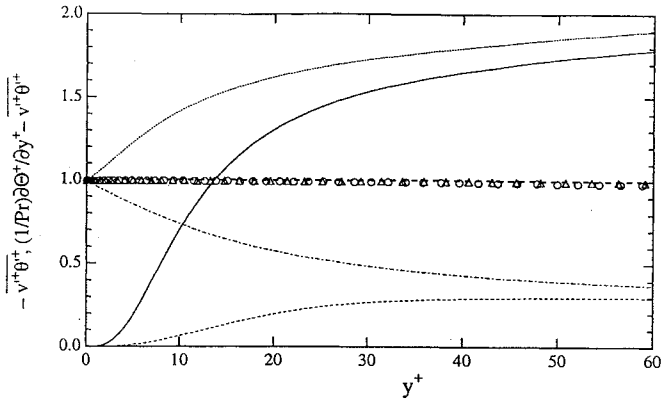

Fig. 11 Component distributions of wall-normal turbulent heat flux. $-\overline{v'^+\theta'^+}$: ——, $F = +0.0034$; - - - - -, $F = -0.0034$; $(1/Pr)\partial\Theta^+/\partial y^+ - \overline{v'^+\theta'^+}$: · · · · · ·, $F = +0.0034$; —·—·—, $F = -0.0034$; $(1/Pr)\partial\Theta^+/\partial y^+ - \overline{v'^+\theta'^+} - v_0^+ \times \Theta^+$: ○, $F = +0.0034$; Δ, $F = -0.0034$.

As seen in Fig. 9, the RHS of Eq. (3) is actually equal to 1 over the channel cross section, and the scalar field is found to be fully developed. The wall-normal turbulent heat flux is remarkably affected by a small amount of fluid injection and suction.

Budgets of Velocity and Temperature Correlations and of Their Destruction Rates

In the fully developed channel flowfield, the budget equation for the turbulent kinetic energy k^+ leads to

$$0 = \underbrace{-V\frac{\partial k}{\partial y}}_{\text{convection}} \underbrace{-\overline{u'v'}\frac{\partial U}{\partial y}}_{\text{production}} \underbrace{-\frac{1}{2}\frac{\partial}{\partial y}\overline{(u_i'u_i'v')}}_{\text{turbulent diffusion}}$$
$$+ \underbrace{\frac{\partial^2 k}{\partial y^2}}_{\text{viscous diffusion}} \underbrace{-\frac{\partial}{\partial y}\overline{(p'v')}}_{\text{pressure diffusion}} \underbrace{-\overline{\frac{\partial u_i'}{\partial x_j}\frac{\partial u_i'}{\partial x_j}}}_{\text{dissipation}} \tag{4}$$

where the subscript $(\,)^+$ is omitted for simplicity and the repeated indices obey the summation convention rule. Figure 12 shows each term included in Eq. (4). The magnitude of each term is markedly larger and smaller on the injection and suction sides, respectively, than that in the case[17] of $F = 0$. With injection, the maximum value of the production term increases by 2.5 times. This must be due to an increase in the Reynolds shear stress $-\overline{u'v'}$. Away from the wall ($y^+ > 30$), the production term balances with the dissipation term. On the suction side, the maximum production rate is only a quarter of that for $F = 0$. The convection term, which is characteristic of the present flowfield, is generally small and only appreciable in the near-wall region; the sign of the term is opposite on the two walls. The pressure diffusion term is negligibly small over the whole cross section.

The transport equation of the dissipation rate of turbulent kinetic energy ε^+ is written as

$$0 = \underbrace{-V\frac{\partial \varepsilon}{\partial y}}_{\text{convection}} \underbrace{-2\overline{\frac{\partial u'}{\partial x_i}\frac{\partial v'}{\partial x_i}\frac{\partial U}{\partial y}}}_{\text{mixed production}} \underbrace{-2\overline{\frac{\partial u_i'}{\partial x}\frac{\partial u_i'}{\partial y}\frac{\partial U}{\partial y}}}_{\text{mean gradient production}}$$
$$\underbrace{-2\overline{v'\frac{\partial u'}{\partial y}\frac{\partial^2 U}{\partial y^2}}}_{\text{gradient production}} \underbrace{-2\overline{\frac{\partial u_i'}{\partial x_j}\frac{\partial u_i'}{\partial x_k}\frac{\partial u_k'}{\partial x_j}}}_{\text{turbulent production}} \underbrace{-\frac{\partial}{\partial y}\overline{\left(v'\frac{\partial u_i'}{\partial x_j}\frac{\partial u_i'}{\partial x_j}\right)}}_{\text{turbulent transport}}$$
$$+ \underbrace{\frac{\partial^2 \varepsilon}{\partial y^2}}_{\text{viscous diffusion}} \underbrace{-2\frac{\partial}{\partial y}\overline{\left(\frac{\partial p'}{\partial x_i}\frac{\partial v'}{\partial x_i}\right)}}_{\text{pressure transport}} \underbrace{-2\overline{\frac{\partial^2 u_i'}{\partial x_j \partial x_k}\frac{\partial^2 u_i'}{\partial x_j \partial x_k}}}_{\text{dissipation}} \tag{5}$$

Each term in Eq. (11) is shown in Fig. 13. On both sides, the gradient production, turbulent transport, pressure transport, and convection

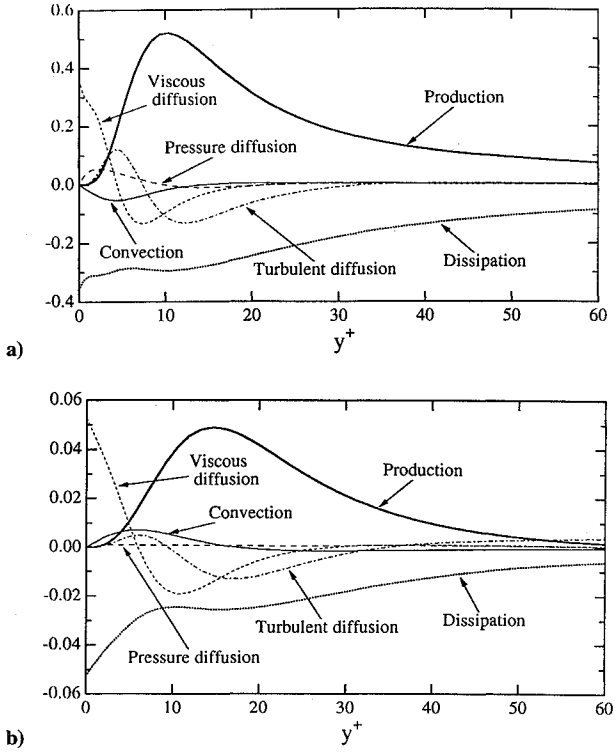

Fig. 12 Budget of turbulent kinetic energy k^+: a) injection side and b) suction side.

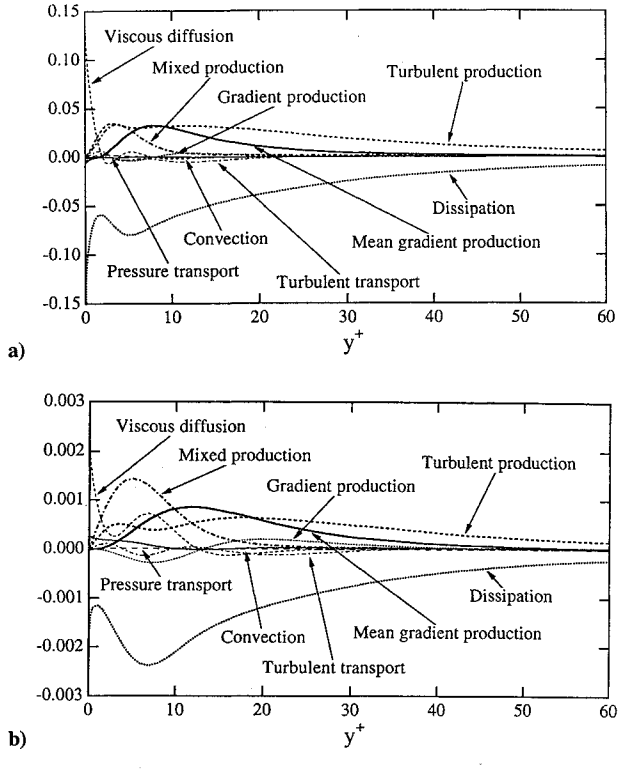

Fig. 13 Budget of kinetic energy dissipation rate ε^+: a) injection side and b) suction side.

terms are negligibly small. The magnitude of each term is again much larger on the injection side and smaller on the suction side. In the vicinity of the wall ($y^+ < 3$), the viscous diffusion term balances with the dissipation term. At $y^+ < 30$, the mixed production, mean gradient production, and turbulent production terms balance with the dissipation term. However, the turbulent production term mainly balances with the dissipation term at $y^+ > 30$ on the injection side and $y^+ > 40$ on the suction side.

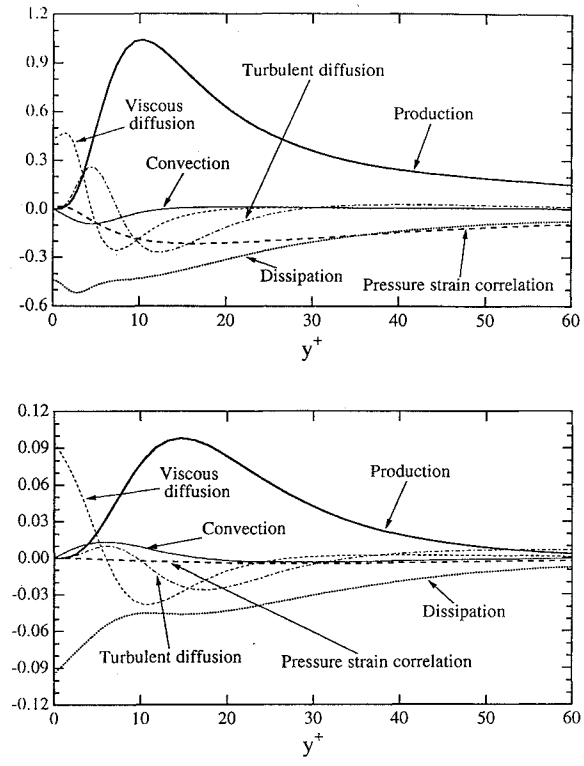

Fig. 14 Budget of the Reynolds normal stress $\overline{u'^2}$: a) injection side and b) suction side.

The transport equation of the Reynolds stresses $-\overline{u_i'^+ u_j'^+}$ is derived as

$$0 = \underbrace{-V\frac{\partial}{\partial y}(\overline{u_i'u_j'})}_{\text{convection}} \underbrace{-\overline{u_i'v'}\frac{\partial \overline{u}_j}{\partial y} - \overline{u_j'v'}\frac{\partial \overline{u}_i}{\partial y}}_{\text{production}} \underbrace{-\frac{\partial}{\partial y}(\overline{u_i'u_j'v'})}_{\text{turbulent diffusion}}$$

$$+ \underbrace{\frac{\partial^2}{\partial y^2}(\overline{u_i'u_j'})}_{\text{viscous diffusion}} + \underbrace{\overline{p'\left(\frac{\partial u_i'}{\partial x_j} + \frac{\partial u_j'}{\partial x_i}\right)}}_{\text{pressure strain correlation}} \underbrace{-\frac{\partial}{\partial y}(\overline{p'u_i'}\delta_{j2} + \overline{p'u_j'}\delta_{2i})}_{\text{pressure diffusion}}$$

$$\underbrace{-2\overline{\frac{\partial u_i'}{\partial x_k}\frac{\partial u_j'}{\partial x_k}}}_{\text{dissipation}} \tag{6}$$

The budget of each Reynolds stress component is successively shown in Figs. 14–17. In general, the magnitude of each term is much larger on the injection side and smaller on the suction side than that with $F = 0$ in Ref. 17. This is in qualitative agreement with the DNS results of turbulent boundary layer with suction in Ref. 14.

In the budget of $\overline{u'^2}$ shown in Fig. 14, the production is a dominant gain term in the region of $y^+ > 5$ on the injection side. The maximum production rate is located at $y^+ = 10$, which is closer to the wall than $y^+ = 12$ for $F = 0$ (see, also, Ref. 16). At $y^+ > 30$, one-half of $\overline{u'^2}$ gained by the production is lost by the dissipation, whereas the other half is redistributed to $\overline{v'^2}$ and $\overline{w'^2}$ through the pressure strain correlation. It is found from comparison with $F = 0$ that the injection should activate this redistribution mechanism. On the suction side, the maximum production is located at $y^+ = 15$, which is shifted a little farther away from the wall. At $y^+ > 30$, the production and dissipation terms mainly balance, but the pressure strain term remains very small. Thus, the suction considerably suppresses the redistribution. The convection term is small and appreciable only at $y^+ < 10$ on both sides.

The budget of $\overline{v'^2}$ is shown in Fig. 15. Note that there is no direct production term for the $\overline{v'^2}$ and $\overline{w'^2}$ components. On the injection side, the pressure strain correlation is negative and balances

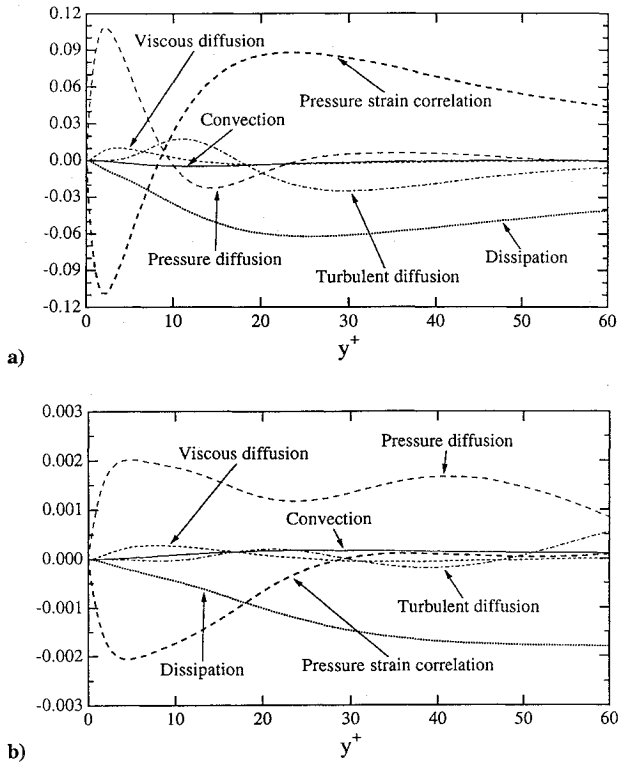

Fig. 15 Budget of the Reynolds normal stress $\overline{v'^{+2}}$: a) injection side and b) suction side.

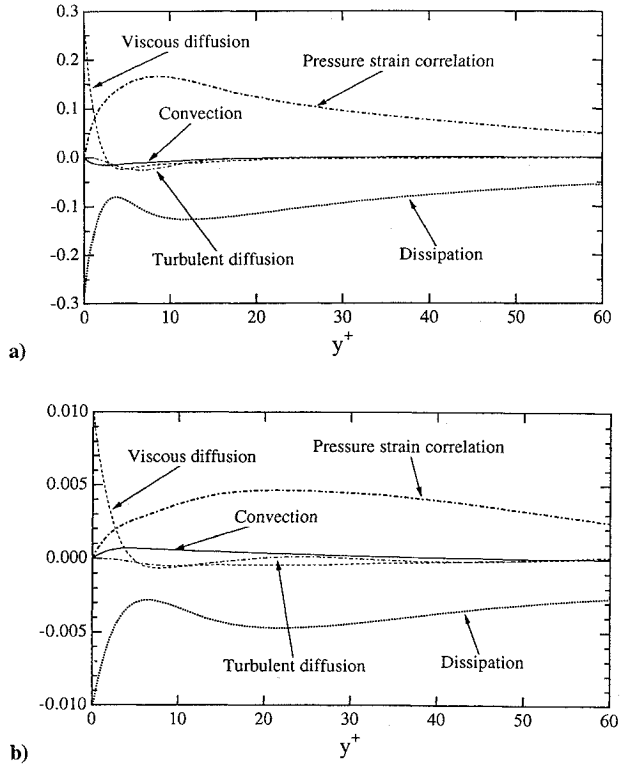

Fig. 16 Budget of the Reynolds normal stress $\overline{w'^{+2}}$: a) injection side and b) suction side.

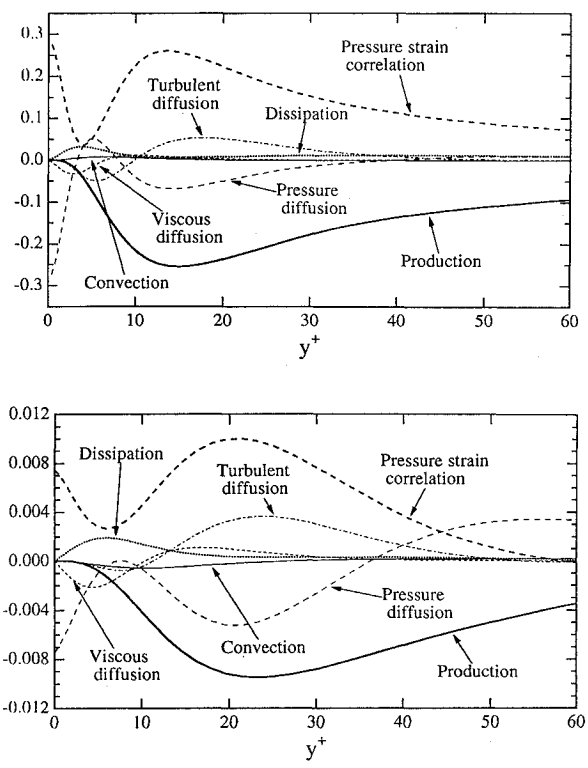

Fig. 17 Budget of the Reynolds shear stress $\overline{u'^{+}v'^{+}}$: a) injection side and b) suction side.

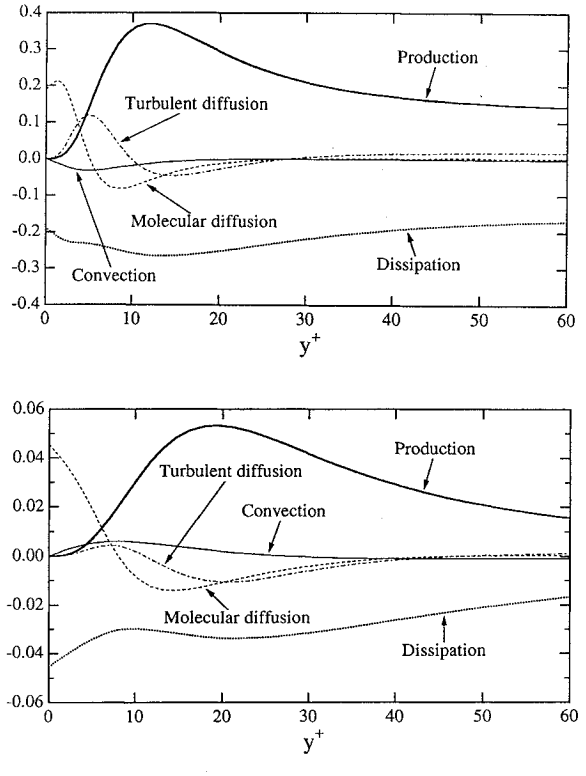

Fig. 18 Budget of the temperature variance k_θ^+: a) injection side and b) suction side.

with the pressure diffusion term at $y^+ < 10$. In this region, the pressure strain term of $\overline{w'^2}$ is positive, as shown later, and, hence, the redistribution even from $\overline{v'^2}$ to $\overline{w'^2}$ takes place. However, at $y^+ > 10$, the pressure strain correlation is positive and balances with the sum of the dissipation and turbulent diffusion terms. Thus, the ordinary redistribution from $\overline{u'^2}$ to $\overline{v'^2}$ and $\overline{w'^2}$ occurs. On the suction side, however, the pressure diffusion is a main gain term, which balances with the pressure strain correlation at $y^+ < 20$ and with the dissipation at $y^+ > 20$. The pressure strain correlation is appreciable only at $y^+ < 30$. On both sides, the viscous diffusion and convection terms are negligibly small.

In Fig. 16, any remarkable change in the budget of $\overline{w'^{+2}}$ cannot be found, although the magnitude of each term is much different, as mentioned previously. In addition, the present budgets on the two walls are qualitatively quite similar. The pressure strain correlation and dissipation terms are dominant except for at the region very close to the wall.

The budget of the Reynolds shear stress $\overline{u'^+v'^+}$ is shown in Fig. 17. As a whole, the effect of injection and suction on this quantity seems much stronger than that on each of the normal stresses. The convection term is again negligibly small over the whole cross section. On the injection side, the production term becomes larger due to an increase in the wall-normal velocity fluctuation $\overline{v'^2}$. Away from the wall ($y^+ > 35$), the production and pressure strain correlation terms are dominant. The dissipation and viscous diffusion terms are negligibly small except in the vicinity of the wall. On the suction side, the wall-normal velocity fluctuation is reduced and, thus, the production term is also suppressed. The pressure strain correlation is still a major sink term, but diminishes rapidly beyond $y^+ > 40$.

The transport equation of the temperature variance k_θ^+ leads to

$$0 = \underbrace{-V\frac{\partial k_\theta}{\partial y}}_{\text{convection}} \underbrace{-\overline{v'\theta'}\frac{\partial \Theta}{\partial y}}_{\text{production}} \underbrace{-\frac{1}{2}\frac{\partial}{\partial y}\overline{(\theta'^2 v')}}_{\text{turbulent diffusion}} + \underbrace{\frac{1}{Pr}\frac{\partial^2 k_\theta}{\partial y^2}}_{\text{molecular diffusion}} \underbrace{-\frac{1}{Pr}\overline{\frac{\partial\theta'}{\partial x_i}\frac{\partial\theta'}{\partial x_i}}}_{\text{dissipation}} \tag{7}$$

Figure 18 shows each term in Eq. (7). In general, the magnitude of each term is larger on the injection side, although smaller on the suction side. On the suction side, the turbulent diffusion term is small. This suggests that the velocity and temperature fluctuations are suppressed by suction, and the temperature variance is diffused mainly by the molecular diffusion term. The maximum production on the injection side is 7 times larger than that on the suction side, and this is because the wall-normal turbulent heat flux on the former is about 6 times larger than that on the latter.

The equation of the dissipation rate of temperature variance ε_θ^+ is written as

$$0 = \underbrace{-V\frac{\partial \varepsilon_\theta}{\partial y}}_{\text{convection}} \underbrace{-\frac{2}{Pr}\overline{\frac{\partial v'}{\partial x_i}\frac{\partial\theta'}{\partial x_i}\frac{\partial\Theta}{\partial y}}}_{\text{mixed production}} \underbrace{-\frac{2}{Pr}\overline{\frac{\partial\theta'}{\partial x}\frac{\partial\theta'}{\partial y}\frac{\partial U}{\partial y}}}_{\text{mean gradient production}}$$
$$\underbrace{-\frac{2}{Pr}\overline{v'\frac{\partial\theta'}{\partial y}\frac{\partial^2\Theta}{\partial y^2}}}_{\text{gradient production}} \underbrace{-\frac{2}{Pr}\overline{\frac{\partial\theta'}{\partial x_i}\frac{\partial\theta'}{\partial x_j}\frac{\partial u_i'}{\partial x_j}}}_{\text{turbulent production}} \underbrace{-\frac{1}{Pr}\frac{\partial}{\partial y}\overline{\left(v'\frac{\partial\theta'}{\partial x_i}\frac{\partial\theta'}{\partial x_i}\right)}}_{\text{turbulent transport}}$$
$$+ \underbrace{\frac{1}{Pr}\frac{\partial^2\varepsilon_\theta}{\partial y^2}}_{\text{molecular diffusion}} \underbrace{-\frac{2}{Pr^2}\overline{\frac{\partial^2\theta'}{\partial x_i\partial x_j}\frac{\partial^2\theta'}{\partial x_i\partial x_j}}}_{\text{dissipation}} \tag{8}$$

The various terms in Eq. (8) are shown in Fig. 19. On the injection side, the gradient production, turbulent transport, viscous diffusion, and convection terms are all negligibly small, and the three remaining terms, i.e., the mean gradient production, turbulent production, and dissipation terms, are dominant. The turbulent production is relatively larger than the mean gradient production on the injection side but not on the suction side. The turbulent production becomes a dominant gain term and balances with the dissipation term at $y^+ > 20$ on the injection side, but only at $y^+ > 50$ on the suction side.

The budget equation of the turbulent heat fluxes $\overline{u_i'^+\theta'^+}$ is derived as

$$0 = \underbrace{-V\frac{\partial}{\partial y}\overline{(u_i'\theta')}}_{\text{convection}} \underbrace{-\overline{u_i'v'}\frac{\partial\Theta}{\partial y} - \overline{v'\theta'}\frac{\partial\overline{u_i}}{\partial y}}_{\text{production}} \underbrace{-\frac{\partial}{\partial y}\overline{(\theta' u_i' v')}}_{\text{turbulent diffusion}}$$
$$+ \underbrace{\frac{\partial}{\partial y}\left(\overline{\theta'\frac{\partial u_i'}{\partial y}} + \frac{1}{Pr}\overline{u_i'\frac{\partial\theta'}{\partial y}}\right)}_{\text{molecular diffusion}} + \underbrace{\overline{p'\frac{\partial\theta'}{\partial x_i}}}_{\text{pressure–temperature gradient correlation}} \underbrace{-\frac{\partial}{\partial x_i}\overline{(p'\theta')}}_{\text{pressure diffusion}}$$
$$\underbrace{-\left(1+\frac{1}{Pr}\right)\overline{\frac{\partial\theta'}{\partial x_j}\frac{\partial u_i'}{\partial x_j}}}_{\text{dissipation}} \tag{9}$$

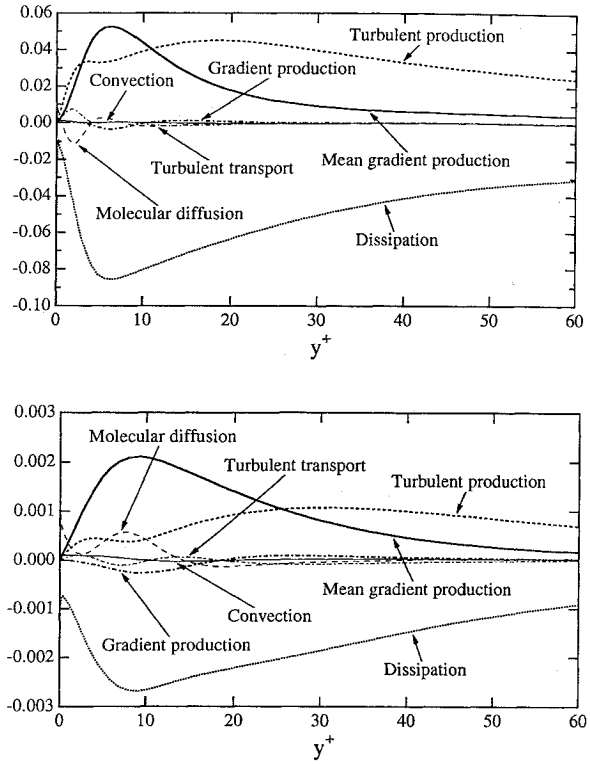

Fig. 19 Budget of the dissipation rate ε_θ^+: a) injection side and b) suction side.

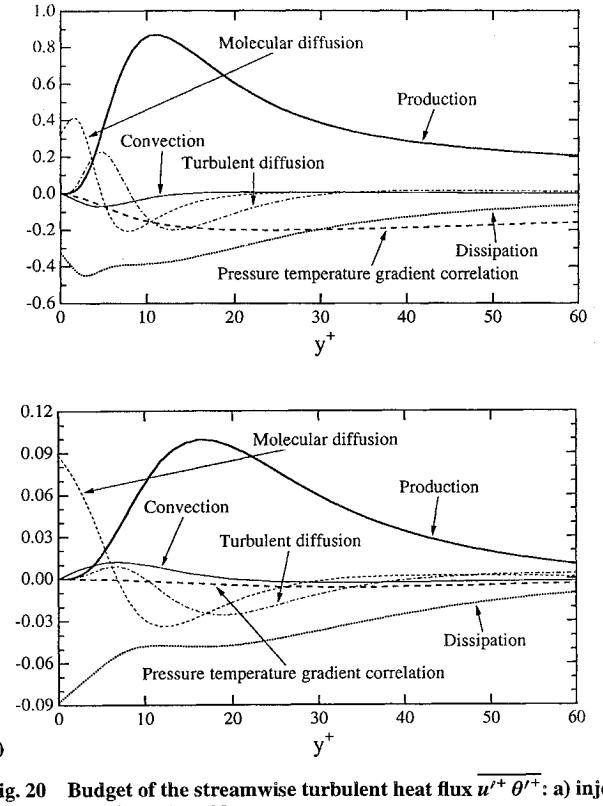

Fig. 20 Budget of the streamwise turbulent heat flux $\overline{u'^+\theta'^+}$: a) injection side and b) suction side.

The budget of the streamwise heat flux $\overline{u'^+\theta'^+}$ is shown in Fig. 20. It is noted that the pressure-temperature gradient correlation is a large loss term on the injection side, although negligibly small on the suction side. On the injection side, the production term balances with the sum of the pressure-temperature gradient correlation term and the dissipation term at $y^+ > 30$, whereas on the suction side the production term balances with the dissipation term at $y^+ > 35$.

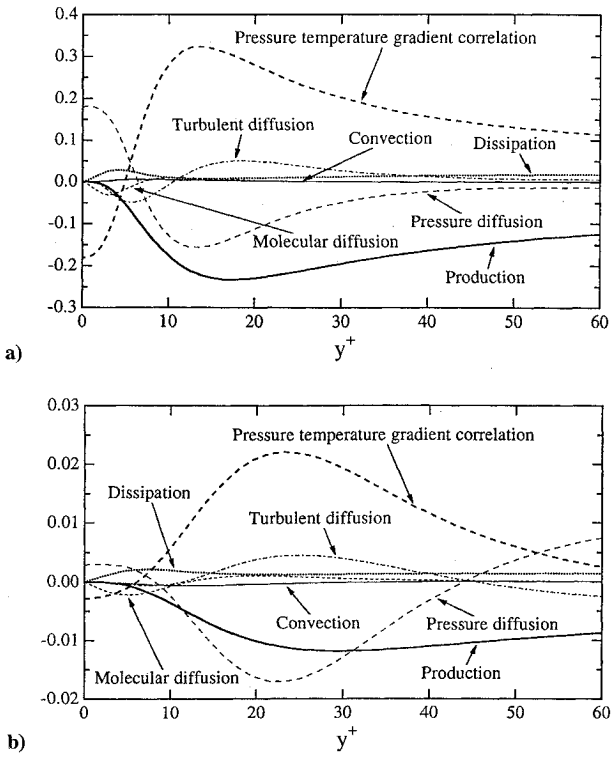

Fig. 21 Budget of the wall-normal turbulent heat flux $\overline{v'^+\theta'^+}$: a) injection side and b) suction side.

The budget of the wall-normal heat flux $\overline{v'^+\theta'^+}$ is shown in Fig. 21. The pressure diffusion and pressure-temperature gradient correlation terms in the near-wall region ($y^+ < 10$) on the injection side are larger than those on the suction side. At $y^+ > 5$ on the injection side, the pressure-temperature gradient correlation term balances with the sum of the production and pressure diffusion terms, whereas farther away from the wall ($y^+ > 40$) the pressure diffusion gradually diminishes. The production term is increased by injection and decreased by suction because $\overline{v'^2}$ is influenced in the same way. On the suction side, the relatively large pressure diffusion term changes its sign around at $y^+ = 45$. On both sides, the molecular diffusion, dissipation, and convection terms are negligibly small.

Near-Wall Quasicoherent Turbulent Structures

Finally, instantaneous flowfields are visualized to investigate how the near-wall turbulence structures are affected by injection and suction. The subvolume visualized has a dimension of about 800, 150, and 400 (ν/u_τ) in the x, y, and z directions, respectively, and is about 1/14 of the total computational domain. It was recently reported that the locally low-pressure regions correspond well to the coherent turbulent vortex cores in wall shear turbulence which generate most of the high Reynolds stress events, the ejection and sweep, around them.[19,20] Kasagi et al.[21] visualized the low-pressure regions in a DNS database[17] of channel flow and also found that many of the low-pressure regions were actually created by intense rotational fluid motions in large scales and associated with the diffusion, redistribution, and destruction mechanisms of Reynolds stresses. Thus, the turbulence mechanisms are coherently and intermittently distributed in space. The three-dimensional contour surfaces of pressure fluctuation at $p'/(p'_{\rm rms})_{\rm max} = -1.7$ in the case without injection and suction are shown in Fig. 22, where the grid spacing is $30(\nu/u_\tau)$, and the lower grid plane corresponds to the bottom wall. The mean flow direction is from the lower left to the upper right. In this figure, typical banana-shaped inclined streamwise vortices, which have been observed most frequently in the near-wall region,[21] are found. Figures 23a and 23b represent the contour surfaces at $p'/(p'_{\rm rms})_{\rm max} = -1.7$ on the injection and suction sides, respectively, in the present flowfield. The grid spacing here is 30 wall units based on the friction velocity at each wall. On the injection side, the

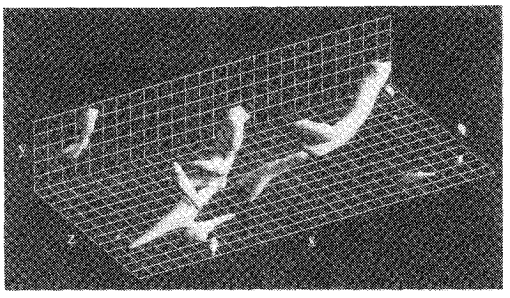

Fig. 22 Three-dimensional contour surfaces of pressure fluctuation, $p'/(p'_{\rm rms})_{\rm max} = -1.7$, in channel flow without wall mass flux.

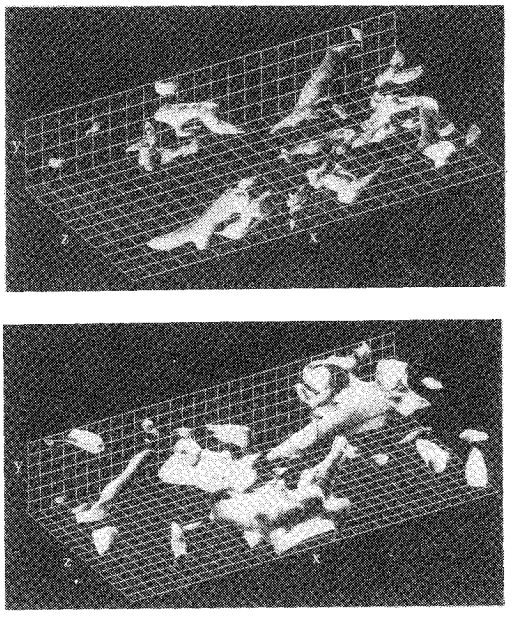

Fig. 23 Three-dimensional contour surfaces of pressure fluctuation, $p'/(p'_{\rm rms})_{\rm max} = -1.7$, in channel flow with injection and suction: a) injection side and b) suction side.

streamwise vortical structures are observed more frequently but in smaller scales; whereas on the suction side, they appear vaguely and in larger scales. Thus, the injection stimulates the occurrence of the coherent streamwise vortical structures and then the production and redistribution of Reynolds stresses, whereas the suction tends to damp the vortical structures.

Conclusions

A direct numerical simulation of the fully developed two-dimensional turbulent channel flow with uniform wall injection and suction between two isothermal walls was carried out, and various low and thermal turbulence statistics and their budgets were calculated. The following conclusions are derived.

1) In accordance with the previous experimental knowledge, with a small amount of wall mass flux, the mean velocity and temperature profiles become asymmetric with respect to the channel centerline, and the friction coefficient as well as the Nusselt number are considerably decreased by injection, although increased by suction.

2) In general, the wall injection tends to activate the near-wall turbulence, whereas the suction suppresses it. As a result, the velocity and temperature fluctuations, the Reynolds shear stress, and the turbulent heat fluxes should increase with injection and decrease with suction.

3) The detailed budgets of turbulent kinetic energy, its dissipation rate, Reynolds stresses, temperature variance, its dissipation rate, and turbulent heat fluxes are calculated. Although the structure of each budget does not exhibit much qualitative difference, the magnitude of each term is generally larger on the injection wall and smaller on the suction wall than that on the ordinary nonpermeable

wall. The convection term, which reflect a direct influence of injection and suction, is very small in every budget examined, and it is mainly through the production and redistribution mechanisms that the injection and suction should markedly affect the turbulent flow and thermal fields. In particular, the pressure strain correlation term of $\overline{v'^2}$, which is the major gain term for this component, shows much different behavior on the injection and suction walls; the injection promotes the intertransfer of turbulent kinetic energy from $\overline{u'^2}$ to $\overline{v'^2}$, whereas the suction attenuates it.

4) The injection stimulates the occurrence of the quasicoherent streamwise vortical structures, which are associated with the primary turbulence mechanisms; on the other hand, the suction considerably suppresses their activities.

Acknowledgment

This work was supported through the Grant-in-Aid for Priority Areas 05240103 by the Ministry of Education, Science and Culture.

References

[1]Bushnell, D. M., and McGinley, C. B., "Turbulence Control in Wall Flows," *Annual Review of Fluid Mechanics*, edited by J. L. Lumley, M. Van Dyke, and H. L. Reed, Annual Reviews Inc., Palo Alto, CA, Vol. 21, 1989, pp. 1–20.

[2]Moffat, R. J., and Kays, W. M., "A Review of Turbulent-Boundary-Layer Heat Transfer Research at Stanford, 1958–1983," *Advances in Heat Transfer*, edited by J. P. Hartnett and T. F. Irvine, Jr., Academic Press, Orlando, FL, Vol. 16, 1984, pp. 241–365.

[3]Hefner, J. N., and Bushnell, D. M., "Viscous Drag Reduction via Surface Mass Injection," *Viscous Drag Reduction in Boundary Layers*, edited by D. M. Bushnell and J. N. Hefner, Vol. 123, Progress in Astronautics and Aeronautics, AIAA, Washington, DC, 1990, pp. 457–476.

[4]Torii, K., Nishiwaki, N., and Hirata, M., "Heat Transfer and Skin Friction in Turbulent Boundary Layer With Mass Injection," *Proceedings of the 3rd International Heat Transfer Conference* (Chicago, IL), AIChE, New York, Vol. 3, 1966, pp. 34–48.

[5]Simpson, R. L., Moffat, R. J., and Kays, W. M., "The Turbulent Boundary Layer on a Porous Plate: Experimental Skin Friction with Variable Injection and Suction," *International Journal of Heat and Mass Transfer*, Vol. 12, No. 7, 1969, pp. 771–789.

[6]Julien, H. L., Kays, W. M., and Moffat, R. J., "Experimental Hydrodynamics of the Accelerated Turbulent Boundary Layer With and Without Mass Injection," *Journal of Heat Transfer*, Vol. 93, Nov. 1971, pp. 373–379.

[7]Anderson, P. S., Kays, W. M., and Moffat, R. J., "Experimental Results for the Transpired Turbulent Boundary Layer in an Adverse Pressure Gradient," *Journal of Fluid Mechanics*, Vol. 69, Pt. 2, May 1975, pp. 353–375.

[8]Kays, W. M., and Moffat, R. J., "The Behavior of Transpired Turbulent Boundary Layers," Stanford Univ., Rept. HMT-20, Stanford, CA, April 1975.

[9]Antonia, A. A., and Fulachier, L., "Topology of a Turbulent Boundary Layer With and Without Wall Suction," *Journal of Fluid Mechanics*, Vol. 198, Jan. 1989, pp. 429–451.

[10]Schildknecht, M., Miller, J. A., and Meier, G. E. A., "The Influence of Suction on the Structure of Turbulence in Fully Developed Pipe Flow," *Journal of Fluid Mechanics*, Vol. 90, Pt. 1, Jan. 1979, pp. 67–107.

[11]Moin, P., "Numerical Simulation of Wall-Bounded Turbulent Shear Flows," *Proceedings of the 8th International Conference on Numerical Methods in Fluid Dynamics*, edited by E. Krause, Springer-Verlag, New York, 1982, pp. 55–76.

[12]Piomelli, U., "Models for Large Eddy Simulations of Turbulent Channel Flows Including Transpiration," Ph.D. Thesis, Stanford Univ., Stanford, CA, Dec. 1987.

[13]Piomelli, U., Ferziger, J., Moin, P., and Kim, J., "New Approximate Boundary Conditions for large Eddy Simulations of Wall-Bounded Flows," *Physics of Fluids*, Vol. A1, No. 6, 1989, pp. 1061–1068.

[14]Mariani, P., Spalart, P., and Kollmann, W., "Direct Simulation of a Turbulent Boundary Layer with Suction," *Near-Wall Turbulent Flows*, edited by R. M. C. So, C. G. Speziale, and B. E. Launder, Elsevier, Amsterdam, 1993, pp. 347–356.

[15]Kim, J., Moin, P., and Moser, R., "Turbulence Statistics in Fully Developed Turbulent Channel Flow at Low Reynolds Number," *Journal of Fluid Mechanics*, Vol. 177, April 1987, pp. 133–166.

[16]Kasagi, N., Tomita, Y., and Kuroda, A., "Direct Numerical Simulation of Passive Scalar Field in a Turbulent Channel Flow," *Journal of Heat Transfer*, Vol. 114, No. 3, 1992, pp. 598–606.

[17]Kuroda, A., Kasagi, N., and Hirata, M., "Direct Numerical Simulation of Turbulent Plane Couette-Poiseuille Flows: Effect of Mean Shear Rate on the Near Wall Turbulence Structures," *Turbulent Shear Flows IX*, edited by F. Durst, N. Kasagi, B. E. Launder, F. W. Schmidt, K. Suzuki, and J. H. Whitelaw, Springer-Verlag, Berlin (to be published, 1994).

[18]Kays, W. M., and Crawford, M. E., *Convective Heat and Mass Transfer*, 2nd ed., McGraw-Hill, New York, 1980, pp. 252–256.

[19]Robinson, S. K., "The Kinematics of Turbulent Boundary Layer Structure," NASA TM-103859, April 1991.

[20]Kasagi, N., and Ohtsubo, Y., "Direct Numerical Simulation of Low Prandtl Number Thermal Field in a Turbulent Channel Flow," *Turbulent Shear Flows VIII*, edited by F. Durst, R. Friedrich, B. E. Launder, F. W. Schmidt, U. Schumann, and J. H. Whitelaw, Springer-Verlag, Berlin, 1993, pp. 97–119.

[21]Kasagi, N., Sumitani, Y., Suzuki, Y., and Iida, O., "On the Kinematics of the Quasi-Coherent Vortical Structure in Near-Wall Turbulence," *International Journal of Heat and Fluid Flow*, Vol. 16, No. 1 (to be published, 1995).